applied optics

Experimental demonstration of square Fresnel zone plate with chiral side lobes

A. Vijayakumar,[1] B. Vinoth,[2] Igor V. Minin,[3] Joseph Rosen,[1,*] Oleg V. Minin,[4] and Chau-Jern Cheng[2]

[1]Department of Electrical and Computer Engineering, Ben-Gurion University of the Negev, P.O. Box 653, Beer-Sheva 8410501, Israel
[2]Institute of Electro-Optical Science and Technology, National Taiwan Normal University, Taipei 11677, Taiwan
[3]Tomsk Politechnic University, 30 Lenina Avenue, 634050 Tomsk, Russia
[4]Tomsk State University, 36 Lenin Avenue, 634050 Tomsk, Russia
*Corresponding author: physics.vijay@gmail.com

Received 1 December 2016; revised 20 February 2017; accepted 20 February 2017; posted 23 February 2017 (Doc. ID 281937); published 17 March 2017

In this study, we introduce what we believe is a novel holographic optical element called a chiral square Fresnel zone plate (CSFZP). The chirality is imposed on a square Fresnel zone plate (SFZP) using a nonclassical technique by rotating the half-period zones relative to one another. The rotation of the half-period zones, in turn, twists the side lobes of the diffraction pattern without altering the focusing properties inherent to a SFZP. As a consequence, the beam profile is hybrid, consisting of a strong central Gaussian focal spot with gradient force similar to that generated by a lens and twisted side lobes with orbital angular momentum. The optical fields at the focal plane were calculated and found to possess a whirlpool-phase profile and a twisted intensity profile. Analysis of the field variation along the direction of propagation revealed a spiraling phase and amplitude distribution. Poynting vector plot of the fields revealed the presence of angular momentum in the regions of chiral side lobes. The phase of the CSFZPs were displayed on a phase-only reflective spatial light modulator and illuminated using a laser. The intensity patterns recorded in the experiment match the calculated ones, with a strong central focal spot and twisted side lobes. The beam pattern was implemented in an optical trapping experiment and was found to possess particle trapping capabilities.

OCIS codes: (090.2890) Holographic optical elements; (090.1760) Computer holography; (050.0050) Diffraction and gratings; (090.1970) Diffractive optics.

https://doi.org/10.1364/AO.56.00F128

1. INTRODUCTION

In 1968, Letokhov proposed that light beams could be used to trap atoms [1]. In 1970, Ashkin discovered that laser light has the ability to apply forces on particles and can trap them [2]. Such optical trapping can be achieved either by using a tightly focused Gaussian-like beam using the gradient force of the intensity profile [2], or by a vortex-like beam with orbital angular momentum [3–5]. The vortex beam is reported to possess many advantages over Gaussian beams in trapping mesoscopic [6] and low-index particles [7]. The generation of radially polarized vortex beam [8] and tunable vortex beams [9] has also been reported to possess interesting optical trapping characteristics. There are other optical beams with interesting intensity and phase profiles such as higher-order Bessel beams [10], which are used for optical trapping applications.

Holographic optical elements (HOEs) such as spiral phase plates [11], forked gratings [12], etc., and axicons [13] are used for the generation of vortex beams and Bessel beams, respectively. For generation of special trapping beams with interesting and useful intensity and phase profiles, such as higher-order Bessel beams [14], flower-shaped beams [15], asymmetric vortex beams [16], focused vortex beams [17], it is necessary to multiplex functions of two or more HOEs or by using refractive/diffractive optical components in tandem. However, the generation of these special beams by such integration of diffractive optical elements always comes with several penalties [18].

Recently, a special type of beam with a central Gaussian peak surrounded by a twisted intensity profile was generated by superposition of a regular Gaussian beam with a vortex beam [19]. This special feature may allow trapping in a larger spatial region, unlike conventional trapping, where the spot has to be overlapped with the particle at least partially in order to trap it. In contrast with the interference method, here we offer the realization of simple HOEs that enable the generation of such special beams with a central Gaussian peak and chiral side lobes in a compact optics configuration. This is done using a square Fresnel zone plate (SFZP) with zone rotation principle and constructive interference, which was proposed for far-field

antennas with chiral beam patterns [20]. SFZP is a simple optical element for light focusing [21]. Optimization of the zone structure for SFZP was discussed [22]. SFZP with a spiral phase was used for generating zero axial irradiance [23]. The chiral beam-pattern formation in far-field microwave antennas was proposed based on rotation of Fresnel zones for SFZP. It has been shown that this principle allows optimizing the side lobe structure of the antenna and the gain [20,24,25]. This principle later was applied to optical vortices generation by binary phase square spiral zone plate [26]. In the current paper, we present a family of simple diffractive optical elements with chiral symmetry of side lobes consisting of both the gradient force at the center as well as orbital angular momentum, which might be useful, for example, for particle trapping applications.

2. METHODOLOGY

The chiral square Fresnel zone plates (CSFZPs) are designed with periodic rotation of zones of SFZP with respect to one another and do not involve any type of multiplexing with other phase functions, and therefore retain their efficiency and prevent any subwavelength features in the design [18,27]. Besides, the generation does not require any refractive/diffractive optical element in tandem to generate the hybrid beam, which makes the optics configuration compact. In general, the light focused by a SFZP has a strong central intensity spot and side lobes focused as line intensity profiles oriented along the horizontal and vertical directions perpendicular to the sides of the SFZP [28]. The periodic rotation of zones twists the side lobes generated at the focal plane of SFZP and redirects the flow of the field to spiral around the central spot. In this way, the beam generated by the CSFZP possesses both the gradient force at the central spot and the orbital angular momentum surrounding it.

For analysis, CSFZPs were designed with a focal length of $f = 60$ cm and with a diameter of $D = 8$ mm for a wavelength of $\lambda = 632.8$ nm. The size of every zone is estimated using the equation of the Fresnel zone plate (FZP) as $Wn = (n^2\lambda^2 + 2nf\lambda)^{1/2}$, where n is the zone number and $n = 0, , 1, \ldots$. The CSFZPs were constructed by rotating the consecutive zones by a fixed angle. The angle of rotation is given by $\theta = Km$, where $m = 2n$ and K is the angular step size. The CSFZPs were designed with binary phase values of 0 and π to obtain the maximum efficiency (40%) possible with any binary profile [29]. The transverse and longitudinal diffraction profiles of the CSFZPs were analyzed using the scalar diffraction formula [29].

The CSFZPs are designed for $K = 1°$ to $8°$ in steps of $2°$, and the corresponding transverse intensity and phase profiles for $z = 60$ cm are computed by computer simulation and are shown in Fig. 1. The order of chirality is defined as the number of curves in the element, and in this case, the order $n = 4$ corresponding to the four vertices of the SFZP. The number of lobes in the diffraction pattern is twice that of n [30], and hence the diffraction pattern shows eight lobes. The transverse phase profiles have a whirlpool-type configuration possessing the possibility for application in optical trapping, and for inducing rotation [31]. The beam profile at the focal plane has a strong central Gaussian peak and chiral

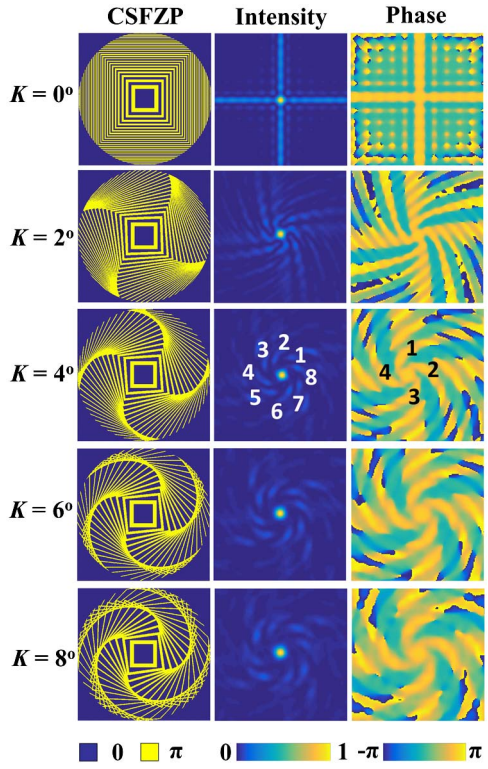

Fig. 1. Images of the CSFZPs designed for a focal length of 60 cm and a wavelength of 632.8 nm; their simulated intensity and phase profiles at the focal plane. The eight side lobes in the intensity profile and the four side lobes in the phase profile are shown for case $K = 4°$.

side lobes. The longitudinal intensity profiles for $z = 40$–80 cm for $K = 0°$ to $8°$ in steps of $2°$ are shown in Fig. 2. From the transverse and longitudinal intensity profiles, it can be noted that even though the zones were rotated, there is no shift in the focal plane. Hence, the element behaves as a lens with a well-defined focal length. The rotation of the zones

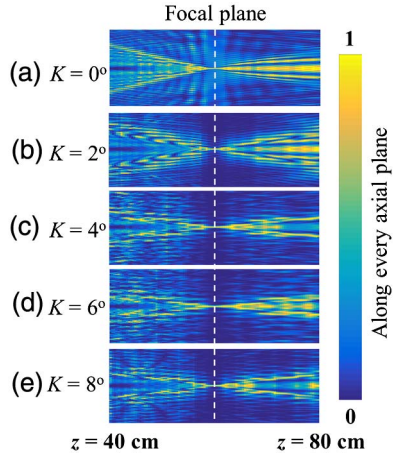

Fig. 2. Axial irradiance profiles of CSFZPs over a distance from 40–80 cm for (a) $K = 0°$, (b) $K = 2°$, (c) $K = 4°$, (d) $K = 6°$, and (e) $K = 8°$. The variation of the intensity and phase profiles for $K = 4°$ is given in Visualization 1 and Visualization 2, respectively.

influences only the profile of the side lobes without altering its focusing characteristics. Therefore, it is possible to implement the CSFZPs for optical trapping applications by matching the trapping plane with the focal plane of the elements.

The normalized intensity profile along the axial direction is analyzed by computer simulation and plotted for $K = 0°$ to $8°$ in steps of $2°$, as shown in Fig. 3(a). The focal depth of the CSFZPs seems to increase with the increase in the zone rotation, indicating the redistribution of intensity from the focal plane to other axial planes. The normalized intensity profile along the transverse direction is compared for different values of K (=0° to 8° in steps of 2°), as shown in Fig. 3(b). An increase of the width of the focal spot can be seen corresponding to the increase in rotation of the zones. The above two effects: increase in focal depth and broadening of the focal spot, arise due to the breakage of symmetry of the SFZP structure because of the rotation of the zones. The beam profile is further analyzed by interfering the diffracted wave at the focal plane with a plane wavefront. The interference patterns for $K = 0°$ to $8°$ are shown in Fig. 4, which shows that there are four dominant lobes equal to the vertices of the zone plate, and the lobes twist and broaden with the increase in the rotation angle of the zones. The variation of the intensity and phase of the field shows the presence of angular momentum.

The presence of orbital angular momentum was verified by studying the Poynting vector plots of the fields generated by the CSFZP. In the case of scalar optical beam, the Poynting vector field is proportional to the product of the gradient of the phase of the beam and its intensity [32,33]. The Poynting vector fields were calculated for two cases: $K = 0°$ and $K = 2°$, as shown in Figs. 5(a) and 5(b), respectively. In both cases, there is a strong gradient force at the center, which is indicated by the lengthier arrows. In the case of CSFZP with $K = 0°$, there is a gradient force along the horizontal and vertical side lobes, while there is an orbital angular momentum seen surrounding the central spot in the case of CSFZP with $K = 2°$. The above analysis confirms the hybrid nature of the optical beam. Similar Poynting vector fields were seen for different values of K.

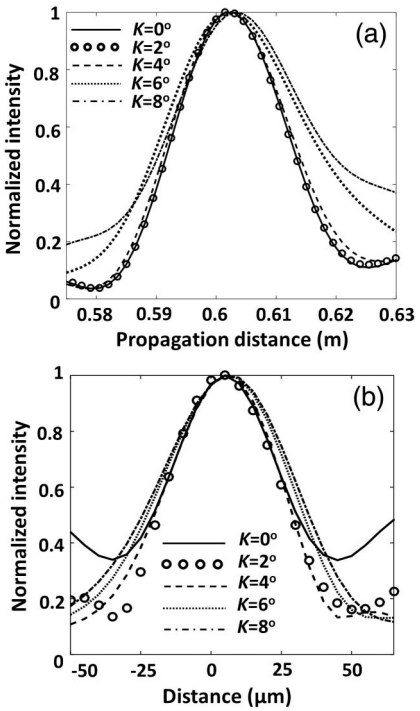

Fig. 3. (a) Normalized plots of the axial intensity profile from 57 cm to 63 cm generated by the CSFZPs for $K = 0°$ (solid line), $K = 2°$ (o), $K = 4°$ (dashed line), $K = 6°$ (dotted line), and $K = 8°$ (dashed and dotted line) and (b) normalized intensity plots of the focal spot generated by the CSFZPs for $K = 0°$ (solid line), $K = 2°$ (o), $K = 4°$ (dashed line), $K = 6°$ (dotted line), and $K = 8°$ (dashed and dotted line).

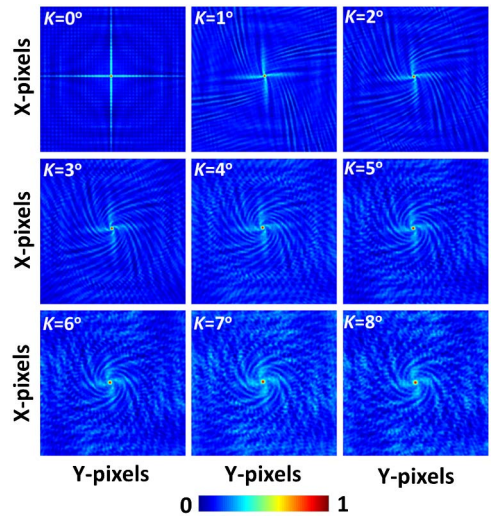

Fig. 4. Interference patterns simulated at the focal plane by superposition of a plane wave with the field diffracted from the CSFZP.

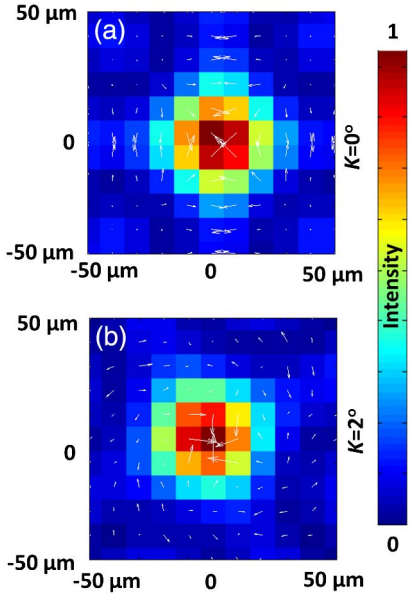

Fig. 5. Poynting vector field plots for the beams generated by the CSFZP for (a) $K = 0°$ and (b) $K = 2°$.

3. EXPERIMENTS

The experimental verification was carried out using a setup as shown in Fig. 6. A He–Ne laser with a wavelength of 632.8 nm was used. The light from the laser was spatial filtered and collimated using lens L_1. A polarizer is used to orient the light parallel to the active axis of a spatial light modulator (SLM) to enable full modulation. The collimated light is projected on the SLM (Holoeye PLUTO, 1920 pixels × 1080 pixels, 8 μm pixel pitch, phase-only modulation). The CSFZPs were displayed on the central part of the SLM with 1000 pixels × 1000 pixels, while the rest are zero padded such that the diameters of the CSFZPs are 8 mm. A camera (Hamamatsu ORCA-Flash4.0 V2 Digital CMOS, 2048 pixels × 2048 pixels, 6.5 μm pixel pitch, monochrome) was mounted at a distance of 60 cm from the SLM. The intensity profiles generated by the CSFZPs with $K = 0°$–$8°$ in steps of 2°, recorded at the focal plane by the camera, are shown in Fig. 7. It can be seen that the experimental results match well with the simulated results. The side lobes of the intensity profile generated by CSFZP without any zone rotation ($K = 0°$) exhibits no twisting similar to Fig. 1. With an increase in the angle of rotation of the zones for $K = 2°$ to 8°, the side lobes of the intensity patterns twist around the central maximum, as shown in Fig. 1. Also from Fig. 7, it can be clearly seen that by increasing the K factor, the side lobes separate from the main lobe, and a chiral structure of focusing beam is formed.

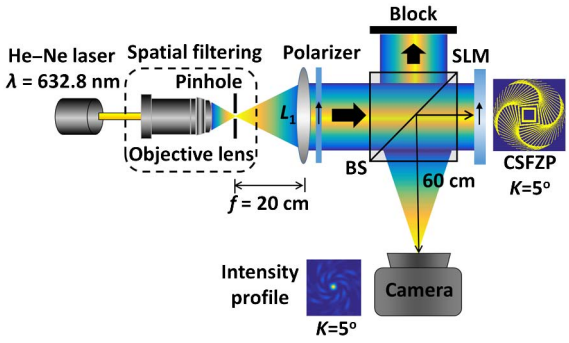

Fig. 6. Experimental set up used for evaluating the far-field diffraction patterns of CSFZPs.

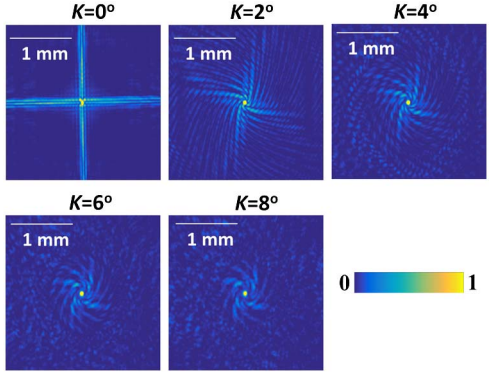

Fig. 7. Experimental intensity patterns recorded at a distance of $z = 60$ cm from the SLM for $K = 0°$–$8°$ in steps of 2°.

The full width at half-maximum (FWHM) of the main lobe in Fig. 7 is about 64 μm for $K = 0°$, and it increases slightly with the zone rotation angle with about 76 μm for $K = 8°$. The FWHM increased by ∼19%, which is close to the increase of 18% as shown in the simulation results of Fig. 3(b). The maximal intensity of vortex side lobes in the image plane are about 12% of the maximal intensity of the central lobe, while it was close to 10% in the simulation. In general, the diffractive optical elements that generate the special optical trapping beams do not possess the necessary numerical aperture (NA) for trapping, and the intensity profiles need to be reimaged using a high NA objective lens [34].

The optical tweezer setup consists of two laser sources with wavelengths $\lambda_1 = 532$ nm (high power laser) and $\lambda_2 = 632.8$ nm for trapping and imaging, respectively. The schematic of the experimental optical tweezer setup is shown in Fig. 8. The spatially filtered light from the green laser source is collimated and is incident on a reflective phase-only SLM (Jasper Display Corp: pixel number: 1920 × 1024; pixel pitch: 6.4 μm) at an angle of 12° (normal incidence requires an additional beam splitter and results in power loss); this angle can be varied from 1° to 15°, which is the acceptance angle of SLM. After SLM, a 4F system is used followed by a 100 × objective lens (NA = 1.3). We have used *Candida rugosa* (ATCC 200555) as a specimen for trapping, and it is recorded by an imaging system. The imaging system consists of a spatial

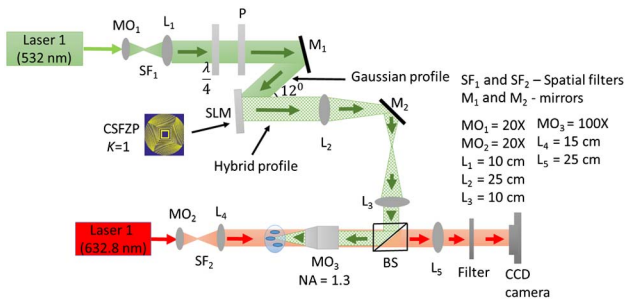

Fig. 8. Schematic of the optical tweezer setup.

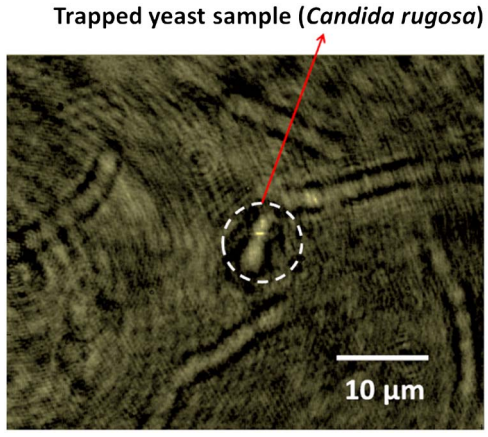

Fig. 9. Optical trapping of *Candida rugosa* with the beam pattern generated by CSFZP for $K = 1°$ (Visualization 3).

filter, 4F imaging system, and a CMOS camera (Thorlabs: pixel number: 1024 × 1280; pixel pitch: 5.2 μm). The phase profiles of the CSFZPs were adjusted to yield maximum efficiency for the trap beam. The specimen was successfully trapped using the beam generated by the CSFZPs. The phase profiles of the CSFZPs were displayed on the phase-only SLM, and the beam generated at its focal plane was reimaged using a 4F optical system to achieve tight focusing of light. The image of the trapping of *Candida rugosa* (ATCC 200555) samples with the beam pattern for ($K = 1°$) is shown in Fig. 9.

4. SUMMARY AND CONCLUSIONS

In conclusion, we experimentally demonstrated a novel family of simple diffractive optical elements called a CSFZP for hybrid beam generation. The chirality is imposed on a SFZP by rotating each half-period zone relative to its neighbor. It has been shown that the rotation of the half-period zones twists the side lobes of the diffraction pattern without altering the transverse focusing properties inherent to a SFZP much, whereas there was a redistribution of intensity from the focal plane to other axial planes, resulting in an increase of the focal depth with the increase in K. The optical fields at the focal plane were calculated and found to possess a whirlpool-phase profile and a twisted intensity profile. The analysis of the variation of the transverse intensity and phase profile revealed rotation of the field with the propagation distance. Hence, this special beam possesses a central strong Gaussian peak with a gradient force, with chiral side lobes with orbital angular momentum that is confirmed by the Poynting vector field plots. This hybrid property of the beam profile makes it suitable for optical trapping applications [35]. The intensity patterns recorded in the experiment are matched with the calculated ones. The CSFZPs were integrated into a standard optical trapping setup, and a preliminary optical trapping experiment was carried out with *Candida rugosa* (ATCC 200555) samples, and the elements were found to possess optical trapping capabilities. The concept has been demonstrated using a square zone plate with a chirality of order four. However, the technique can be extended to design elements with lower or higher chirality order by decreasing or increasing the number of vertices of the zone plate, respectively.

In the current demonstration, an SLM is used for displaying the CSFZPs in order to generate the special beams with chiral side lobes. However, SLMs in general have a relatively low resolution of around 10 μm and interpixel gaps. Since the quality of the beam depends upon the resolution of the HOE [18], for applications such as optical trapping [34], it is desirable to employ passive HOEs fabricated using high-resolution lithography techniques [17,27]. The phase profile of the FZP can also be modified to cancel the central peak to obtain vortex-like beams. The concept is presented with a FZP, while the design can be tailored for different applications by replacing FZP with a Fresnel zone axilens [36] or axicons [37] and also with other useful diffractive optical elements. CZFZPs are designed with binary phase profiles, and therefore can exhibit a maximum efficiency of only 40%. Higher efficiency can be obtained by designing a multilevel version of the CSFZP. However, fabrication of such blazed structures is a challenging task [17,27]. The intensity and phase profiles generated by the CSFZPs can also be useful for communications and optical vortex microscopy [38].

Funding. Israel Science Foundation (ISF) (439/12); Ministry of Science, Technology and Space; Ministry of Science and Technology, Taiwan (MOST) (MOST 102-2221-E-003 -025 -MY3); Russian Foundation for Basic Research (RFBR) (17-02-00132); Mendeleev Scientific Fund of Tomsk State University (8.2.48.2015).

REFERENCES

1. V. S. Letokhov, "The narrowing of Doppler broadened line in standing light wave," Pis'ma Zh. Eksp. Teor. Fiz. **7**, 348–351 (1968) [JETP Lett. 7, 272 (1968)].
2. A. Ashkin, "Acceleration of trapping of particles by radiation pressure," Phys. Rev. Lett. **24**, 156–159 (1970).
3. X. Yuan, B. S. Ahluwalia, W. C. Cheong, L. Zhang, J. Bu, S. Tao, K. J. Moh, and J. Lin, "Micro-optical elements for optical manipulation," Opt. Photon. News **17**(7), 36–41 (2006).
4. V. Arrizón, U. Ruiz, D. Sánchez-de-la-Llave, G. Mellado-Villaseñor, and A. S. Ostrovsky, "Optimum generation of annular vortices using phase diffractive optical elements," Opt. Lett. **40**, 1173–1176 (2015).
5. I. Augustyniak, A. Popiołek-Masajada, J. Masajada, and S. Drobczyński, "New scanning technique for the optical vortex microscope," Appl. Opt. **51**, C117–C124 (2012).
6. J. Ng, Z. Lin, and C. T. Chan, "Theory of optical trapping by an optical vortex beam," Phys. Rev. Lett. **104**, 103601 (2010).
7. K. T. Gahagan and G. A. Swartzlander, "Trapping of low-index microparticles in an optical vortex," J. Opt. Soc. Am. B **15**, 524–534 (1998).
8. M. Beresna, M. Gecevičius, P. G. Kazansky, and T. Gertus, "Radially polarized optical vortex converter created by femtosecond laser nanostructuring of glass," Appl. Phys. Lett. **98**, 201101 (2011).
9. M. Gecevičius, R. Drevinskas, M. Beresna, and P. G. Kazansky, "Single beam optical vortex tweezers with tunable orbital angular momentum," Appl. Phys. Lett. **104**, 231110 (2014).
10. K. Volke-Sepulveda, V. Garcés-Chávez, S. Chávez-Cerda, J. Arlt, and K. Dholakia, "Orbital angular momentum of a high-order Bessel light beam," J. Opt. B **4**, S82–S89 (2002).
11. W. G. Cheong, W. M. Lee, X.-C. Yuan, L.-S. Zhang, K. Dholakia, and H. Wang, "Direct electron-beam writing of continuous spiral phase plates in negative resist with high power efficiency for optical manipulation," Appl. Phys. Lett. **85**, 5784–5786 (2004).
12. N. R. Heckenberg, R. McDuff, C. P. Smith, and A. G. White, "Generation of optical phase singularities by computer-generated holograms," Opt. Lett. **17**, 221–223 (1992).
13. V. Garcés-Chávez, D. Roskey, M. D. Summers, H. Melville, D. McGloin, E. M. Wright, and K. Dholakia, "Optical levitation in a Bessel light beam," Appl. Phys. Lett. **85**, 4001–4003 (2004).
14. A. Vasara, J. Turunen, and A. T. Friberg, "Realization of general nondiffracting beams with computer-generated holograms," J. Opt. Soc. Am. A **6**, 1748–1754 (1989).
15. A. Vijayakumar and S. Bhattacharya, "Compact generation of superposed higher-order Bessel beams via composite diffractive optical elements," Opt. Eng. **54**, 111310 (2015).
16. B. Zhang and D. Zhao, "Focusing properties of Fresnel zone plates with spiral phase," Opt. Express **18**, 12818–12823 (2010).
17. A. Vijayakumar and S. Bhattacharya, "Design, fabrication, and evaluation of a multilevel spiral-phase Fresnel zone plate for optical trapping," Appl. Opt. **51**, 6038–6044 (2012).
18. A. Vijayakumar and S. Bhattacharya, "Design of multifunctional diffractive optical elements," Opt. Eng. **54**, 024104 (2015).
19. P. Vaity and L. Rusch, "Perfect vortex beam: Fourier transformation of a Bessel beam," Opt. Lett. **40**, 597–600 (2015).
20. I. V. Minin and O. V. Minin, *Basic Principles of Fresnel Antenna Arrays* (Springer, 2008).
21. L. J. Janicijevic, "Diffraction characteristics of square zone plates," J. Opt. **13**, 199–206 (1982).

22. I. V. Minin, O. V. Minin, A. Petosa, and S. Thirakoune, "Improved zoning rule for designing square Fresnel zone plate lenses," Microw. Opt. Technol. Lett. **49**, 276–278 (2007).
23. B. Zhang and D. Zhao, "Square Fresnel zone plate with spiral phase for generating zero axial irradiance," Opt. Lett. **35**, 1488–1490 (2010).
24. I. V. Minin, O. V. Minin, E. G. Danilov, and G. S. Lbov, "Parameters optimization algorithm of a new type of diffraction optics elements," in *Proceedings of 5th IEEE-Russia Conference on Microwave Electronics: Measurement, Identification, Applications (MEMIA)* (2005), pp. 177–185.
25. I. V. Minin and O. V. Minin, "Array of Fresnel zone plate lens antennas: circular, hexagonal with chiral symmetry and hexagonal boundary," in *Digest of the Joint 31st International Conference on Infrared and Millimeter Waves and 14th International Conference on Terahertz Electronics* (2006), p. 270.
26. N. Gao, C. Xie, C. Li, C. Jin, and M. Liu, "Square optical vortices generated by binary spiral zone plates," Appl. Phys. Lett. **98**, 151106 (2011).
27. A. Vijayakumar, M. Uemukai, and T. Suhara, "Phase-shifted Fresnel zone lenses for photomixing generation of coherent THz wave," Jpn. J. Appl. Phys. **51**, 070206 (2012).
28. J. Alda, J. M. Rico-Garcia, F. J. Salgado-Remacha, and L. M. Sanchez-Brea, "Diffractive performance of square Fresnel zone plates," Opt. Commun. **282**, 3402–3407 (2009).
29. B. C. Kress and P. Meyrueis, *Applied Digital Optics* (Wiley, 2009).
30. N. Jiménez, R. Picó, V. Sánchez-Morcillo, V. Romero-García, L. M. García-Raffi, and K. Staliunas, "Formation of high-order acoustic Bessel beams by spiral diffraction gratings," arXiv.org/abs/1604.08353 (2016).
31. U. S. Kivshar and E. A. Ostrovskaya, "Optical vortices folding and twisting waves of light," Opt. Photon. News **12**(4), 24–28 (2001).
32. V. Kumar and N. K. Viswanathan, "Topological structures in the Poynting vector field: an experimental realization," Opt. Lett. **38**, 3886–3889 (2013).
33. A. Y. Bekshaev and M. S. Soskin, "Transverse energy flows in vectorial fields of paraxial beams with singularities," Opt. Commun. **271**, 332–348 (2007).
34. A. Vijayakumar, P. Parthasarathi, S. S. Iyengar, R. Selvan, S. Ananthamurthy, S. Bhattacharya, and S. Bhattacharya, "Conical Fresnel zone lens for optical trapping," Proc. SPIE **9654**, 965426 (2015).
35. M. Bacia, W. Lamperska, J. Masajada, S. Drobczynski, and M. Marc, "Polygonal micro-whirlpools induced in ferrofluids," Opt. Appl. **45**, 309–316 (2015).
36. N. Davidson, A. A. Friesem, and E. Hasman, "Holographic axilens: high resolution and long focal depth," Opt. Lett. **16**, 523–525 (1991).
37. I. Golub, "Fresnel axicon," Opt. Lett. **31**, 1890–1892 (2006).
38. Ł. Płocinniczak, A. Popiołek-Masajada, J. Masajada, and M. Szatkowski, "Analytical model of the optical vortex microscope," Appl. Opt. **55**, B20–B27 (2016).